A SCOPF model for congestion management considering power flow controlling devices

Abhimanyu Kaushal*†, Hakan Ergun*†
Dirk Van Hertem*†
* KU Leuven ESAT - ELECTA, Belgium
† EnergyVille, Genk, Belgium
{abhimanyu.kaushal, hakan.ergun,
dirk.vanhertem}@kuleuven.be

Evelyn Heylen‡§
‡ Centrica Business Solutions, Belgium
§ Control and Power group,
Imperial College London
{e.heylen}@imperial.ac.uk

***Abstract*—With an increase in the share of distributed renewable generation, the power flow patterns are changing, and there is an increasing probability of internal congestion. There is also an increase in the number of power flow controlling devices in the transmission system to provide greater flexibility to the system operator. Thus, there is a need to include these devices and intra-zonal transmission lines for the congestion management analysis. This paper presents a probabilistic security-constrained optimal power flow (SCOPF) model for congestion management based on the non-linear ac formulation. To ensure computational efficiency, a second-order cone (soc) relaxation for power flow controlling devices is proposed. A comparison between the ac and soc formulations has been carried out on the modified IEEE 118-bus AC/DC system. It is observed that with the soc formulation, the computational efficiency of the model is increased while ensuring a minimal gap between the ac and soc results.**

***Index Terms*—Congestion management, power flow controlling devices, power system operation, security-constrained optimal power flow, second-order cone relaxation.**

NOMENCLATURE

TABLE I: Indices and sets definition

AC branches	$b \in \mathcal{B}$
AC generator connectivity	$gi \in \mathcal{T}^{gen,ac} \subseteq \mathcal{G} \times \mathcal{I}$
AC load connectivity	$li \in \mathcal{T}^{load,ac} \subseteq \mathcal{L} \times \mathcal{I}$
AC nodes	$i,j \in \mathcal{I}$
AC topology	$bij \in \mathcal{T}^{ac} \subseteq \mathcal{B} \times \mathcal{I} \times \mathcal{I}$
AC/DC converters	$c \in \mathcal{C}$
AC/DC converter topology	$cie \in \mathcal{T}^{c} \subseteq \mathcal{C} \times \mathcal{I} \times \mathcal{E}$
Contingencies	$o \in \mathcal{O}$
DC branches	$d \in \mathcal{D}$
DC load connectivity	$le \in \mathcal{T}^{load,dc} \subseteq \mathcal{L} \times \mathcal{E}$
DC nodes	$e,f \in \mathcal{E}$
DC topology	$def \in \mathcal{T}^{dc} \subseteq \mathcal{D} \times \mathcal{E} \times \mathcal{E}$
Generators	$g \in \mathcal{G}$
Loads	$l \in \mathcal{L}$
Phase shifting transformers	$p \in \mathcal{P}$

I. INTRODUCTION

Renewable energy sources (RES) are expected to contribute to 61% of the total generation in Europe by 2040 [1]. Large-scale integration of RES will lead to significant changes in power flows in the system. These power flows would also be highly variable and, in some instances, may also cause loop (transit) flows in the grid. As the power system is typically operated closer to its operational limits, such changes in power flows may lead to grid congestion [2]. It is the responsibility of transmission system operators (TSO) to alleviate the intra-zonal as well as cross-zonal congestion in day-ahead and real-time by applying remedial actions [3]. These could be in the form of costly actions such as rescheduling the generating units as presented in [4]. Alternately, more economical measures such as power flow controlling (PFC) devices (phase-shifting transformers (PSTs), flexible AC transmission systems (FACTS), transformer taps, and high voltage direct current (HVDC) systems) could be utilized to redirect power flows and mitigate congestion [5]. The TSO can choose to apply the remedial actions for congestion management in the operational planning stage, i.e. preventive actions and/or corrective/curative actions that are implemented only in real-time.

The authors in [6] have presented a SCOPF formulation for an AC system that uses generator redispatch and on-load tap changer (OLTC) transformer for congestion management. In [7] the authors have presented the effects of PST on congestion management. The formulation in [8] explores the utilization of HVDC systems and PSTs for congestion management of an AC/DC grid. However, the flexibility of generator curative control actions has not been considered. Moreover, a trade-off between preventive and curative actions is not envisaged. The inclusion of all PFC devices in the preventive-curative SCOPF framework would help quantify the additional flexibility these devices provide in managing congestion and aid the operator in making more cost-effective decisions.

With the above motivation, this paper proposes a preventive-curative SCOPF model with non-linear ac formulation for congestion management of AC/DC grids. The proposed model presents a trade-off between the preventive cost and curative risk associated with various contingencies. This SCOPF model considers the actions of generators and PFC devices (HVDC and PST) with detailed modelling of the PST. As this SCOPF problem is a large-scale non-linear and non-convex optimization problem, it leads to a significant computational time or sub-optimal solution. One available solution to this problem is the dc approximation that does not take reactive power flow and voltage magnitudes into account. However, the authors in [9] and [10] have mentioned that dc approximation has its

limitations, and it provides unrealistic results in some cases. Convex relaxation of the non-linear ac problem can enhance the computational speed while guaranteeing a global optimal solution of the relaxed problem [11]. The authors in [12] and [13] have presented soc relaxation for solving optimal power flow (OPF) for radial and meshed AC networks, respectively. In [14], [15], the authors have presented the soc relaxation for the AC/DC grid OPF problem. They have demonstrated that such a formulation leads to lower computational time than the solution with ac formulation while ensuring a small optimality gap.

Based on the above insights, this paper presents the soc relaxation for the proposed AC/DC grid congestion management SCOPF problem by including the soc constraints for the PST. The outcomes of the soc formulation are bench-marked against the non-linear ac formulation in terms of computation time and the resulting decisions of the PFC devices. The SCOPF model has been implemented in Julia/JuMP [16], [17] as an extension to the existing packages of PowerModels.jl [18], PowerModelsACDC.jl [15], and PowerModelsReliability.jl [19].

The paper is organized as follows. The mathematical model for the optimization problem with non-linear ac formulation is presented in the section II. Section III presents the soc relaxation for the PST. The test system and various considerations for the analysis are presented in section IV. The outcomes for these analyses are discussed in section V and section VI summarizes the conclusions of this paper.

II. SCOPF MODEL FOR CONGESTION MANAGEMENT

In this paper, congestion management has been considered as a two-stage SCOPF optimization problem, with the preventive stage (represented by superscript p), the curative stage (represented by superscript c) being the two stages. The system's optimal active power dispatch state without any contingency has been taken as the starting point for the SCOPF problem and is designated as the reference stage (superscript ref). The SCOPF problem aims to minimize the total operational risk (w.r.t. the reference stage), which leads to social welfare maximization.

The total operational risk represents the sum of the preventive costs and the curative risk. The preventive costs include the redispatch costs for generator actions (ΔP_g^p), converter actions (ΔP_c^p) and PST actions ($\Delta \alpha_p^p$). The curative risk is calculated by weighing the probability of a contingency (π_o) times the total curative costs, summed over all contingencies. The curative costs comprise the costs for generator, converter, and PST curative redispatch actions ($\Delta P_{g,o}^c$, $\Delta P_{c,o}^c$, $\Delta \alpha_{p,o}^c$) and demand curtailment ($\Delta P_{l,o}^c$). The generator redispatch cost coefficients for preventive and curative stage are represented by C_g^p and C_g^c, respectively. The costs associated with changes in converter and PST setpoints for preventive and curative stages are represented by C_c^p, C_p^p, C_c^c and C_p^c respectively. The value of lost load coefficient $VoLL$ is used to account for demand curtailment costs. The absolute value of the respective redispatches has been considered in the objective function. The objective function is given as below:

$$min \Bigg[\sum_g C_g^p \cdot |\Delta P_g^p| + \sum_c C_c^p \cdot |\Delta P_c^p| + \sum_p C_p^p \cdot |\Delta \alpha_p^p| + \sum_o \pi_o \cdot \Bigg(\sum_g C_g^c \cdot |\Delta P_{g,o}^c| + \sum_c C_c^c \cdot |\Delta P_{c,o}^c| + \sum_p C_p^c \cdot |\Delta \alpha_{p,o}^c| + \sum_l VoLL \cdot |\Delta P_{l,o}^c| \Bigg) \Bigg] \quad (1)$$

The individual redispatches are calculated as follows:

$$\Delta P_g^p = P_g^p - P_g^{ref} \ \ \forall \ g \in \mathcal{G} \quad (2)$$
$$\Delta P_c^p = P_c^p - P_c^{ref} \ \ \forall \ c \in \mathcal{C} \quad (3)$$
$$\Delta \alpha_p^p = \alpha_p^p - \alpha_p^{ref} \ \ \forall \ p \in \mathcal{P} \quad (4)$$
$$\Delta P_{g,o}^c = P_{g,o}^c - P_g^p \ \ \forall \ g \in \mathcal{G}, \ \ \forall \ o \in \mathcal{O} \quad (5)$$
$$\Delta P_{c,o}^c = P_{c,o}^c - P_c^p \ \ \forall \ c \in \mathcal{C}, \ \ \forall \ o \in \mathcal{O} \quad (6)$$
$$\Delta P_{l,o}^c = P_{l,o}^c - P_l^{ref} \ \ \forall \ l \in \mathcal{L}, \ \ \forall \ o \in \mathcal{O} \quad (7)$$
$$\Delta \alpha_{p,o}^c = \alpha_{p,o}^c - \alpha_p^p \ \ \forall \ p \in \mathcal{P}, \ \ \forall \ o \in \mathcal{O} \quad (8)$$

The AC system constraints for the SCOPF problem have been considered similar to those in [18]. The constraints for various system elements are as follows:

A. Generators

Generator setpoints are constrained by the respective equipment limits for all stages as given below:

$$\left.\begin{array}{l} \underline{P_g} \le P_g \le \overline{P_g} \\ \underline{Q_g} \le Q_g \le \overline{Q_g} \end{array}\right\} \ \forall \ g \in \mathcal{G} \quad (9)$$

where $\overline{P_g}$, $\underline{P_g}$, $\overline{Q_g}$ and $\underline{Q_g}$ represent the generator active and reactive power limits [20]. The change in generator setpoints for preventive and curative stages are bounded by the following limits:

$$\left.\begin{array}{ll} \underline{P_g} - \overline{P_g} & \le \Delta P_g \le \overline{P_g} - \underline{P_g} \\ \underline{Q_g} - \overline{Q_g} & \le \Delta Q_g \le \overline{Q_g} - \underline{Q_g} \end{array}\right\} \ \forall \ g \in \mathcal{G} \quad (10)$$

B. HVDC converter stations

The steady-state converter station model has been implemented as considered in [15]. The relationship of converter AC side current and converter active and reactive power flow are used as those presented in [21]. The converter DC side current and active power flow follow the same constraints as mentioned in [21].

For the converters, the AC side active and reactive power flows in preventive and curative stages are limited by the operational limits as given below:

$$\left.\begin{array}{l} \underline{P_c^{ac}} \le P_c^{ac} \le \overline{P_c^{ac}} \\ \underline{Q_c^{ac}} \le Q_c^{ac} \le \overline{Q_c^{ac}} \\ (P_c^{ac})^2 + (Q_c^{ac})^2 \le (S_c^{ac,rated})^2 \end{array}\right\} \ \forall \ c \in \mathcal{C} \quad (11)$$

For the DC side of the converters, the active power limits are imposed for all stages as per:

$$\underline{P_c^{dc}} \leq P_c^{dc} \leq \overline{P_c^{dc}} \ \ \forall \ \ c \in \mathcal{C} \tag{12}$$

For the change in converter setpoints for the preventive and curative stages, the following limits have been used:

$$\left.\begin{array}{l} \underline{P_c^{ac}} - \overline{P_c^{ac}} \leq \Delta P_c^{ac} \leq \overline{P_c^{ac}} - \underline{P_c^{ac}} \\ \underline{Q_c^{ac}} - \overline{Q_c^{ac}} \leq \Delta Q_c^{ac} \leq \overline{Q_c^{ac}} - \underline{Q_c^{ac}} \\ \underline{P_c^{dc}} - \overline{P_c^{dc}} \leq \Delta P_c^{dc} \leq \overline{P_c^{dc}} - \underline{P_c^{dc}} \end{array}\right\} \ \forall \ \ c \in \mathcal{C} \tag{13}$$

Converter losses link the converter AC and DC side power flows for all stages and are represented by the model in [15]:

$$P_c^{ac} + P_c^{dc} = P_c^{loss} \ \ \forall \ \ c \in \mathcal{C} \tag{14}$$

C. System nodes

For all system nodes, the nodal power balance equations are fulfilled for all stages of the SCOPF model as per the following:

$$\sum_{cie \epsilon \mathcal{T}^c} P_{cie}^{dc} + \sum_{def \epsilon \mathcal{T}^{dc}} P_{def} = - \sum_{le \epsilon \mathcal{T}^{load,dc}} P_{le} \ \ \forall \ \ e \in \mathcal{E} \tag{15}$$

$$\sum_{cie \epsilon \mathcal{T}^c} P_{cie}^{tf} + \sum_{bij \epsilon \mathcal{T}^{ac}} P_{bij} = \sum_{gi \epsilon \mathcal{T}^{gen,ac}} P_{gi} - \sum_{li \epsilon \mathcal{T}^{load,ac}} P_{li} - g_i^{shunt} (U_i)^2 \ \ \forall \ \ i \in \mathcal{I} \tag{16}$$

$$\sum_{cie \epsilon \mathcal{T}^c} Q_{cie}^{tf} + \sum_{bij \epsilon \mathcal{T}^{ac}} Q_{bij} = \sum_{gi \epsilon \mathcal{T}^{gen,ac}} Q_{gi} - \sum_{li \epsilon \mathcal{T}^{load,ac}} Q_{li} + b_i^{shunt} (U_i)^2 \ \ \forall \ \ i \in \mathcal{I} \tag{17}$$

In (16-17), the converter transformer power flows P_{cie}^{tf} and Q_{cie}^{tf} are considered as the converter is connected to the AC bus at this point as elaborated in [15].

For all the stages, the nodal voltages are subjected to the operational limits as follows:

$$\underline{U_i} \leq U_i \leq \overline{U_i} \ \ \forall \ \ i \in \mathcal{I} \tag{18}$$

$$\underline{U_e} \leq U_e \leq \overline{U_e} \ \ \forall \ \ e \in \mathcal{E} \tag{19}$$

For all the stages, the phase angle difference for the AC nodes is limited as follows:

$$\underline{\theta_{ij}} \leq \theta_{ij} \leq \overline{\theta_{ij}} \ \ \forall \ \ i,j \in \mathcal{I} \tag{20}$$

where $\underline{\theta_{ij}}$ and $\overline{\theta_{ij}}$ are the phase angle difference limits.

D. PST

The PST angle should adhere to the angle limits $\underline{\alpha_p}$ and $\overline{\alpha_p}$ for all the stages:

$$\underline{\alpha_p} \leq \alpha_p \leq \overline{\alpha_p} \ \ \forall \ \ p \in \mathcal{P} \tag{21}$$

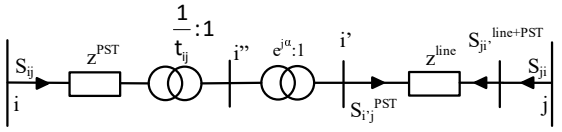

Fig. 1: Equivalent circuit of transmission line with tapable and shiftable transformer

E. System loads

Load-shedding is allowed only in the curative stages as a final countermeasure for reliable system operation. The load setpoints for the curative stages are calculated as given below:

$$\left.\begin{array}{l} \underline{P_l} \leq P_{l,o}^c \leq P_l^{ref} \\ \underline{Q_l} \leq Q_{l,o}^c \leq Q_l^{ref} \end{array}\right\} \ \forall \ \ l \in \mathcal{L}, \ \ o \in \mathcal{O} \tag{22}$$

where $\underline{P_l}$ and $\underline{Q_l}$ are the load minimum active and reactive power limits, respectively. For the curative stages, the demand curtailment is constrained as follows:

$$\left.\begin{array}{l} \underline{P_l} - P_l^{ref} \leq \Delta P_{l,o}^c \leq P_l^{ref} - \underline{P_l} \\ \underline{Q_l} - Q_l^{ref} \leq \Delta Q_{l,o}^c \leq Q_l^{ref} - \underline{Q_l} \end{array}\right\} \forall \ l \in \mathcal{L}, \ o \in \mathcal{O} \tag{23}$$

The load setpoints are adapted in curative stages to maintain the same load power factor as the reference stage as per the following:

$$Q_{l,o}^c = P_{l,o}^c \cdot \frac{Q_l^{ref}}{P_l^{ref}} \ \ \forall \ \ l \in \mathcal{L}, \ \ o \in \mathcal{O} \tag{24}$$

F. DC branches

For the DC branches, the power flow is divided by the number of poles as considered for the single line representation [15]. The power flow constraint for the DC branches are given as:

$$P_{def} + P_{dfe} = P_d^{loss} \ \ \forall \ \ def \in \mathcal{T}^{dc} \tag{25}$$

P_d^{loss} in above, represents the power loss in DC branches. These branch power flows are also limited by the rated limits for all stages and are given by:

$$-P_d^{rated} \leq P_{def} \leq P_d^{rated} \ \ \forall \ \ def \in \mathcal{T}^{dc} \tag{26}$$

G. AC branches

The AC branch power flow equations are considered as detailed in [18] based on Ohm's law and Kirchhoff's Current Law (KCL). A generic model of the AC transmission line is considered as shown in Fig. 1 where the line is connected to an asymmetrical PST (with t_{ij} tap position and α_{ij} phase angle) between nodes i and j. The active and reactive power flows through the line are given by the equations in Table II. g_{ij} and g_{ij}^{sh} in these equations are the branch π section conductance parameters.

TABLE II: Branch power flow equations

$$P_{ij} = (g_{ij} + g_{ij}^{sh}) \cdot \left(\frac{|V_i|}{t_{ij}}\right)^2 - g_{ij} \cdot \frac{|V_i|}{t_{ij}} \cdot |V_j| \cdot cos(\theta_{ij} - \alpha_{ij}) - b_{ij} \cdot \frac{|V_i|}{t_{ij}} \cdot |V_j| \cdot sin(\theta_{ij} - \alpha_{ij})$$

$$Q_{ij} = -(b_{ij} + b_{ij}^{sh}) \cdot \left(\frac{|V_i|}{t_{ij}}\right)^2 + b_{ij} \cdot \frac{|V_i|}{t_{ij}} \cdot |V_j| \cdot cos(\theta_{ij} - \alpha_{ij}) - g_{ij} \cdot \frac{|V_i|}{t_{ij}} \cdot |V_j| \cdot sin(\theta_{ij} - \alpha_{ij})$$

$$P_{ji} = (g_{ij} + g_{ij}^{sh}) \cdot (|V_j|)^2 - g_{ij} \cdot \frac{|V_i|}{t_{ij}} \cdot |V_j| \cdot cos(\alpha_{ij} - \theta_{ij}) - b_{ij} \cdot \frac{|V_i|}{t_{ij}} \cdot |V_j| \cdot sin(\alpha_{ij} - \theta_{ij})$$

$$Q_{ji} = -(b_{ij} + b_{ij}^{sh}) \cdot (|V_j|)^2 + b_{ij} \cdot \frac{|V_i|}{t_{ij}} \cdot |V_j| \cdot cos(\alpha_{ij} - \theta_{ij}) - g_{ij} \cdot \frac{|V_i|}{t_{ij}} \cdot |V_j| \cdot sin(\alpha_{ij} - \theta_{ij})$$

III. SOC RELAXATION FOR PFC DEVICES

In this section, the soc bus injection model for the PST has been presented for the congestion management SCOPF model. The soc relaxation uses lifted variables in place of voltage products of the non-linear power flow constraints, thereby convexifying the same. The equality constraint is thus relaxed into an inequality constraint [22]. The soc relaxation for AC transmission system elements has been presented in [18]. The soc relaxation is formulated in [15] for the HVDC transmission system. In this paper, we have introduced the lifted variables for the PST as shown in Table III. The product of nodal voltages has been linearized by assigning the lifted variable W. Another variable $W_{i"}^{p}$ has been assigned to include the effect of PST taps on the nodal voltage product. Similarly, the variable $W_{i'}^{t,\alpha}$ is used to incorporate the effects of PST tap and angle. Table IV presents the branch power flow equations after the substitution of the lifted variables.

TABLE III: Lifted variables of soc relaxation

$$W_i = |V_i|^2, \quad W_{ij} = |V_i| \cdot |V_j| \qquad (s.1)$$

$$W_{ij}^{R} = |V_i| \cdot |V_j| \cdot cos(\theta_{ij}), \quad W_{ij}^{I} = |V_i| \cdot |V_j| \cdot sin(\theta_{ij})$$

$$W_{i"}^{p} = \frac{W_i}{(t_{ij})^2}, \qquad W_{i'}^{t} = W_{i"}^{p} \cdot cos(\alpha_{ij})^2 = |V_{i'}|^2$$

$$W_{i'j}^{t,I} = cos(\alpha_{ij}) \cdot \frac{W_{ij}^{I}}{t_{ij}}, \qquad W_{i'j}^{t,R} = cos(\alpha_{ij}) \cdot \frac{W_{ij}^{R}}{t_{ij}}$$

$$W_{i'}^{t,\alpha} = (|V_{i'}| \cdot tan(\alpha_{ij}))^2 = W_{i"}^{p} \cdot sin(\alpha_{ij})^2$$

$$W_{i'j}^{t,\alpha,I} = W_{i"j}^{p,R} \cdot sin(\alpha_{ij}), \qquad W_{i'j}^{t,\alpha,R} = W_{i"j}^{p,I} \cdot sin(\alpha_{ij})$$

At the branch terminal nodes, the auxiliary variables linking the voltage magnitudes and angles relate to each other in a quadratic way as follows:

$$(W_{ij}^{R})^2 + (W_{ij}^{I})^2 = W_i \cdot W_j \qquad (27)$$

TABLE IV: Branch power flow equations with soc relaxation

$$P_{ij} = (g_{ij} + g_{ij}^{sh}) \cdot W_{i'}^{t} - g_{ij} \cdot W_{i'j}^{t,R} - b_{ij} \cdot W_{i'j}^{t,I} + (g_{ij} + g_{ij}^{sh}) \cdot W_{i'}^{t,\alpha} - g_{ij} \cdot W_{i'j}^{t,\alpha,R} + b_{ij} \cdot W_{i'j}^{t,\alpha,I}$$

$$Q_{ij} = -(b_{ij} + b_{ij}^{sh}) \cdot W_{i'}^{t} + b_{ij} \cdot W_{i'j}^{t,R} - g_{ij} \cdot W_{i'j}^{t,I} - (b_{ij} + b_{ij}^{sh}) \cdot W_{i'}^{t,\alpha} + b_{ij} \cdot W_{i'j}^{t,\alpha,R} + g_{ij} \cdot W_{i'j}^{t,\alpha,I}$$

$$P_{ji} = (g_{ij} + g_{ij}^{sh}) \cdot W_j - g_{ij} \cdot W_{i'j}^{t,R} + b_{ij} \cdot W_{i'j}^{t,I} - g_{ij} \cdot W_{i'j}^{t,\alpha,R} - b_{ij} \cdot W_{i'j}^{t,\alpha,I}$$

$$Q_{ji} = -(b_{ij} + b_{ij}^{sh}) \cdot W_j + b_{ij} \cdot W_{i'j}^{t,R} + g_{ij} \cdot W_{i'j}^{t,I} + b_{ij} \cdot W_{i'j}^{t,\alpha,R} - g_{ij} \cdot W_{i'j}^{t,\alpha,I}$$

To obtain a convex optimization problem, the convex equality constraint in (27) is relaxed to a convex inequality constraint as given below:

$$(W_{ij}^{R})^2 + (W_{ij}^{I})^2 \leq W_i \cdot W_j \qquad (28)$$

By using bounds on the PST angles which assure that $cos(\alpha_{ij})$ is always positive, the McCormick relaxation [23] has been used to convexify the auxiliary variables with non-negative lower bounds as given in Table V.

TABLE V: McCormick relaxations for auxiliary variables

$$\overline{W_{i"j}^{p,I}} \cdot cos(\alpha_{ij}) + W_{i"j}^{p,I} \cdot \underline{cos(\alpha_{ij})} - \overline{W_{i"j}^{p,I}} \cdot \underline{cos(\alpha_{ij})} \geq W_{i'j}^{t,I}$$

$$W_{i"j}^{p,I} \cdot \overline{cos(\alpha_{ij})} + \underline{W_{i"j}^{p,I}} \cdot cos(\alpha_{ij}) - \underline{W_{i"j}^{p,I}} \cdot \overline{cos(\alpha_{ij})} \geq W_{i'j}^{t,I}$$

$$\underline{W_{i"j}^{p,I}} \cdot cos(\alpha_{ij}) + W_{i"j}^{p,I} \cdot \underline{cos(\alpha_{ij})} - \underline{W_{i"j}^{p,I}} \cdot \underline{cos(\alpha_{ij})} \leq W_{i'j}^{t,I}$$

$$W_{i"j}^{p,I} \cdot \overline{cos(\alpha_{ij})} + \overline{W_{i"j}^{p,I}} \cdot cos(\alpha_{ij}) - \overline{W_{i"j}^{p,I}} \cdot \overline{cos(\alpha_{ij})} \leq W_{i'j}^{t,I}$$

$$\overline{W_{ij}^{I}} \cdot \frac{1}{t_{ij}} + W_{ij}^{I} \cdot \frac{1}{t_{ij}^{max}} - \overline{W_{ij}^{I}} \cdot \frac{1}{t_{ij}^{max}} \geq W_{i"j}^{p,I}$$

$$W_{ij}^{I} \cdot \frac{1}{t_{ij}^{min}} + \underline{W_{ij}^{I}} \cdot \frac{1}{t_{ij}} - \underline{W_{ij}^{I}} \cdot \frac{1}{t_{ij}^{min}} \geq W_{i"j}^{p,I}$$

$$\underline{W_{ij}^{I}} \cdot \frac{1}{t_{ij}} + W_{ij}^{I} \cdot \frac{1}{t_{ij}^{max}} - \underline{W_{ij}^{I}} \cdot \frac{1}{t_{ij}^{max}} \leq W_{i"j}^{p,I}$$

$$W_{ij}^{I} \cdot \frac{1}{t_{ij}^{min}} + \overline{W_{ij}^{I}} \cdot \frac{1}{t_{ij}} - \overline{W_{ij}^{I}} \cdot \frac{1}{t_{ij}^{min}} \leq W_{i"j}^{p,I}$$

Lifted non-linear cuts as used in [24] are used to tighten the relaxations. The relationship of auxiliary variables for the PST to the base variables contains bi-linear terms. The equality constraints for these bi-linear terms with lower non-negative bounds can be replaced by the following convex inequalities:

$$\frac{W_i}{\overline{t_{ij}}^2} \leq W_{i"}^{p} \leq \frac{W_i}{\underline{t_{ij}}^2} \qquad (29)$$

$$\frac{W_i^{R}}{\overline{t_{ij}}} \leq W_{i"}^{p,R} \leq \frac{W_i^{R}}{\underline{t_{ij}}} \qquad (30)$$

$$W_{i"}^{p} \cdot \underline{(cos(\alpha_{ij}))^2} \leq W_{i'}^{t} \leq W_{i"}^{p} \cdot \overline{(cos(\alpha_{ij}))^2} \quad (31)$$

$$W_{i"j}^{p,I} \cdot \overline{cos(\alpha_{ij})} + \overline{W_{i"j}^{p,I}} \cdot cos(\alpha_{ij}) - \overline{W_{i"j}^{p,I}} \cdot \overline{cos(\alpha_{ij})} \leq W_{i'j}^{t,I} \quad (32)$$

IV. Test system and assumptions

The congestion management analysis has been carried out on the IEEE-118 bus system as defined in [25] and modified as per [26]. The transmission line transfer capacity is reduced to 80% of the original capacity. The loads in areas 1 and 2 are increased by 50%, and those in area 3 are increased by 75%. The generator ratings are increased by 25% for all the generators. Using the system data from [25], it was seen that 12 transmission lines were operating at more than 80% of their rated power limits. By installing PSTs on three transmission lines (dotted blue lines in Fig. 2), changing 2 AC transmission lines to HVDC and inclusion of a new HVDC line (red lines in Fig. 2) as suggested in [26], the number of lines with line loading more than 80% is reduced to 6. The installed PSTs have a maximum tap position of $\pm 30°$. It was assumed that the system operates in a secure state for 98% of time, and the remaining 2% of the time was equally divided for all the contingencies. The preventive redispatch cost is taken as 1.5 times the dispatch cost for all generators. The generator curative redisptach cost for different contingencies is taken as five times the dispatch cost [27]. A high demand curtailment cost of 5,000 €/MWh is considered to discourage load shedding and only use it in extreme cases [28]. A nominal cost of 1 €/MW and 1 €/° has been considered in all stages for changes in converter active power setpoints and PST angles, respectively. This cost can be attributed to the wear and tear of the respective equipment. The PST angle change has been considered a continuous variable.

The simulations were performed on a PC of 2.6-GHz and 32-GB RAM. The IPOPT solver [29] and the Gurobi solver [30] were used for analysis with ac and soc formulations, respectively.

V. Results and discussion

In this section, the comparison of both formulations has been done in terms of operational risk, computation time, generator, converter and PST setpoints. The analysis was carried out with different contingency sets as presented in the following sections:

A. Case-1

For validation of the soc formulation and its comparison with the ac formulation, the simulations were performed initially with a set of 3 AC branch contingencies for the considered test system. A comparison of the outcomes of soc formulation and full ac formulation is presented as follows:

1) Operational risk: The ac formulation does not guarantee a global optimal solution, whereas the soc convex relaxation provides a global optimal solution. From the comparison of the system operational risk obtained for both approaches, it is seen that the soc formulation provides a lower risk as compared to the ac formulation, as shown in Table VI. It is observed that with both the formulations, there is no preventive stage cost; however, for ac formulation, redispatch actions are needed in the curative stages. A difference in the branch power flows is observed with the two formulations. Due to this, a redispatch of 9 MW is required for contingency-1 with the ac formulation, whereas for the soc formulation, there is no requirement of generator redispatch. This difference in redispatch volume contributes to the overall difference in the operational risk.

TABLE VI: System operation risk and costs

Parameter Formulation	Total risk [€/h]	Preventive cost [€/h]	Curative risk [€/h]
ac	2.83	0.00	2.83
soc	0.00	0.00	0.00

2) Computation time: The computation time for ac and soc formulation is presented in TableVII, and it can be seen that the computation time with soc is very small as compared to that with full ac formulation. The soc formulation is 100 times faster as compared to the ac formulation for the considered contingency set.

TABLE VII: Computation time

Formulation	ac	soc
Time [s]	67.5	0.67

3) Generator setpoints: It was seen that the generator setpoints for both formulations are similar, with an overall difference of 9 MW (0.15% of total active power dispatch) in generator active power setpoints for all the contingencies. This can be attributed to changed branch power flows due to the different formulations.

4) Converter setpoints: The outcomes for the converter DC side setpoints were seen to be similar with the two formulations. A total difference of 11 MW was observed in the overall converter redispatch volume summed for all the contingencies.

5) PST setpoints: The ac and soc formulation resulted in the same setpoints for all the PSTs for all the considered contingencies.

6) Pf feasibility: The power flow feasibility of soc results was checked by carrying out ac power flow analysis based on soc results for the generator, converter and PST setpoints. It was seen that the ac power flow converges for each of the contingencies based on the soc results. No AC and DC nodal voltage violations (v_{ac}^{v} and v_{dc}^{v}) were observed while carrying out the ac power flow analysis. For the AC branches, an average branch power flow violation (v_{ac}^{s}) of 0.2 MVA was observed for only 1.2% of the branches and for DC branches, no power flow violation (v_{dc}^{p}) was observed.

With the above comparison, it was seen that the soc formulation provides similar results to that from the ac formulation.

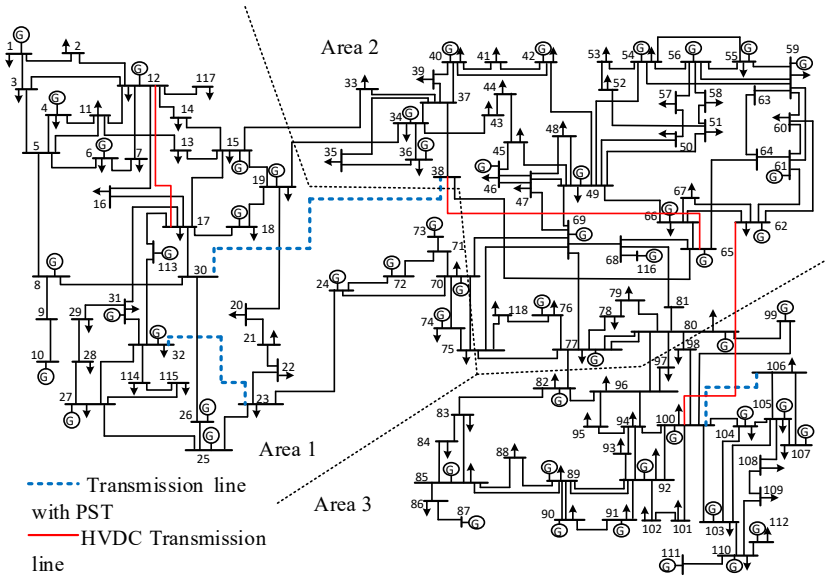

Fig. 2: Modified IEEE-118 bus system [25] [26]

B. Case-2

To further check the applicability of soc formulation, a set of 10 branch contingencies (10 system states represented by $o1 - o10$) was considered for detailed comparison with ac formulation. The results of this comparison are presented below:

1) Operational risk: From the comparison of the system operational risk obtained for both approaches, it can be seen that the soc formulation provides a lower risk as compared to the ac formulation, as shown in Table VIII. With both the formulations, no preventive stage redispatch actions are needed, and only curative redispatch is utilized. The gap between the hourly operational risk with two approaches (ac-soc) is € 26.8, which is $\sim 29\%$ of the hourly operational risk with the ac formulation.

TABLE VIII: System operation risk and costs

Parameter / Formulation	Total risk [€/h]	Preventive cost [€/h]	Curative risk [€/h]
ac	93.99	0.00	93.99
soc	67.14	0.00	67.14

Fig. 3 shows the costs associated with system operation for various system states. The overall generator dispatch cost for both formulations is comparable, as shown in Fig. 3a. However, the soc formulation results in a lower redispatch cost as compared to the ac formulation, as is evident from Fig. 3b.

2) Computation time: The computation time for ac and soc formulation is compared in Table IX, and it can be seen that the computation time with soc has been reduced by a factor of ~ 400 as compared to that with ac formulation.

3) Generator setpoints: As there is no preventive redispatch for the system operation, the preventive stage generator setpoints are same with the two formulations.

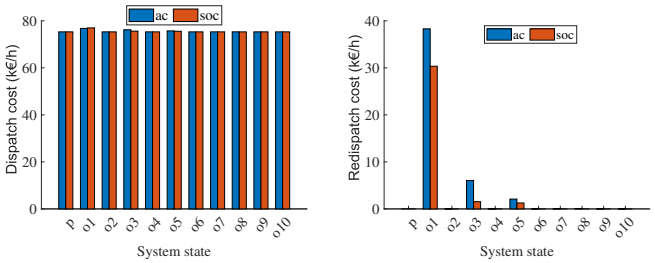

(a) Dispatch cost (b) Redispatch cost

Fig. 3: Costs associated with system operation

TABLE IX: Computation time

Formulation	ac	soc
Time [s]	971.45	2.45

The average and maximum difference (ac-soc) (only the absolute values have been considered) in generator setpoints for ac and soc formulations for various system states can be seen in Fig. 4. It can be observed from Fig. 4a that the average difference in generators' setpoints is negligible for system states except for $o1$, $o3$ and $o5$. Even for these three system states, the average difference in active power setpoints is very small (< 4 MW). The maximum difference in generators' active power setpoints is presented in Fig. 4b. As there is no difference in generator setpoints for the system states (except for $o1$, $o3$ and $o5$), the maximum active power difference is also negligible. The maximum difference of ~ 70 MW in generators' active power setpoints was observed for system state $o1$.

4) Converter setpoints: There was no difference in converter setpoints for the preventive stage for both the formulations. The average and maximum difference (ac-soc) (for the absolute values) in converter setpoints for all system states

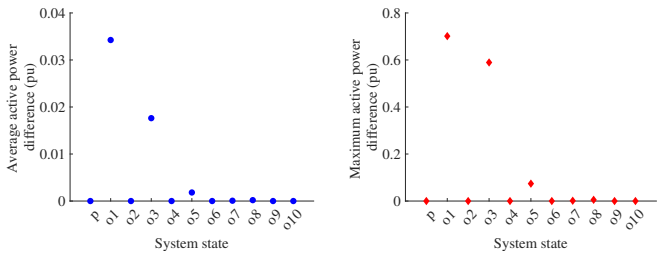

(a) Average difference (b) Maximum difference

Fig. 4: Difference in generator setpoints

is presented in Fig. 5. The values in Fig. 5 are represented with 100 MW base. For the converters also, it was seen that there is no difference in setpoints for system states except for $o1$, $o3$ and $o5$. The maximum average difference (< 40 MW) in converter setpoints was observed for $o3$ system state. The maximum difference of ~ 100 MW in converter setpoints was also observed for the same system state.

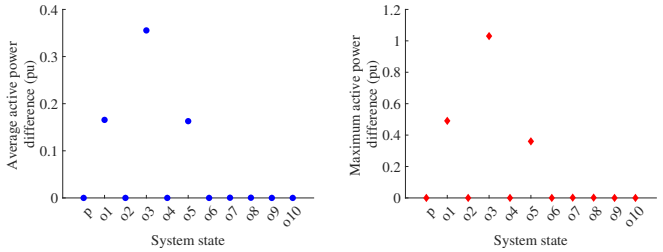

(a) Average difference (b) Maximum difference

Fig. 5: Difference in converter setpoints

5) PST setpoints: The setpoints for the three PSTs for all system states and for both formulations are shown in Fig. 6. For system states $o1$, $o3$ and $o5$; there is some difference in PST2 setpoints, whereas, for other system states, the PST setpoints are similar. The average difference in PST angle for all three PSTs for all system states and for ac and soc formulation comes out to be $\sim 1°$.

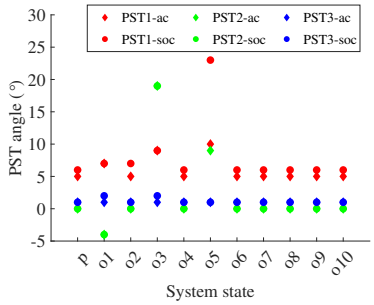

Fig. 6: PST setpoints for different system states

6) Pf feasibility: Similar to Case-1, the ac power flow feasibility analysis was carried out for the soc results of Case-2. It was seen that for the system states $o1$, $o3$, and $o5$, the ac power flow did not converge; however, for the remaining system states, the ac power flow converged and resulted in a feasible solution. For the ac power flow feasible solutions, no v^p_{dc} was observed for DC branches. For 17 AC branches (for all system states combined), an average v^s_{ac} of 0.18 MVA was observed. For all system states, an average v^v_{dc} of 0.01 pu was observed for a total of 18 DC nodes for all ac feasible soc solutions. No v^v_{ac} was observed for the soc solutions. The summary of power flow feasibility analysis is presented in Table X.

TABLE X: Pf feasibility check for soc solutions for case-2

Violation	v^s_{ac}	v^v_{ac}	v^p_{dc}	v^v_{dc}
No. of violations (%)	1.15	0	0	5.6
Average value	0.18 MVA	0	0.01 pu	0

Detailed analysis was carried out for system states $o1$, $o3$ and $o5$ to investigate the difference in ac and soc formulation results and for non-convergence of ac power flow. It was seen that there is a difference in branch power flows for these formulations. Due to this difference in power flows, the generators' dispatch and redispatch setpoints are different for ac and soc formulations which lead to variation in dispatch, redispatch cost and converter and PST setpoints.

As the soc formulation relaxes the bounds of the optimization problem, in some cases, it is seen that the results obtained with soc formulation are outside the bounds for ac formulation by a small margin. To identify the binding constraints which are resulting in infeasible ac power flow solution, the bounds for various system constraints were relaxed. It was seen that when the ac nodal voltage bounds were relaxed by $\pm 2\%$ from the initial range of 0.94-1.06 pu, the ac power flow converged for $o1$ and $o5$ system states. For system state $o3$, the ac power flow convergence was obtained on relaxing the ac nodal voltage bounds by $\pm 5\%$.

C. Case-3

For checking the scalability of the soc formulation, further analysis was carried out for congestion management by considering all possible branch contingencies. For this 175 transmission lines (excluding radial lines and lines with PFC devices) were selected. With ac formulation, the full-scale N-1 analysis was not feasible. The N-1 analysis was feasible with the soc formulation while considering 165 transmission lines contingencies. The total computation time for the simulation was 181s. On checking the ac power flow feasibility of the soc results, the ac power flow converged for 150 soc solutions. The outcomes of power flow feasibility analysis are as shown in Table XI. For the feasible ac power flow solutions, an average v^s_{ac} of 0.09 MVA was observed for 1.09% of AC branches (for all system states combined). No v^v_{ac} and v^p_{dc} were observed for ac nodal voltage and power flow on DC branches. Average v^v_{dc} of 0.02 pu was observed for 64% of the system DC nodes for all ac feasible soc solutions.

VI. CONCLUSION

This paper proposes a probabilistic preventive-curative SCOPF model for congestion management considering the

TABLE XI: Pf feasibility check for Case-3 soc results

Violation	v^s_{ac}	v^v_{ac}	v^p_{dc}	v^v_{dc}
No. of violations (%)	1.09	0	0	64
Average value	0.09 MVA	0	0	0.02 pu

flexibility of PFC devices. The soc formulation for the phase-shifting transformer has been presented and compared with the non-linear ac formulation. From the case studies on the modified IEEE-118 bus system, it was seen that the soc formulation offers increased computational efficiency as the computation time is reduced by a factor of $\sim$ 400. The generator, converter and PST setpoints obtained from the soc formulation were found to be comparable to that of the ac formulation. For some contingencies, there was a difference in the soc and the ac results. Detailed analysis showed that this difference originates due to the difference in branch power flows with the soc formulation, which leads to a different dispatch/redispatch in the respective contingency states. The proposed soc SCOPF formulation was also applied to a full N-1 analysis, wherein it was found to be computationally efficient while ensuring ac power flow feasibility for the majority of the system states. From the analysis, it can be concluded that the proposed soc formulation can be used in place of the full ac formulation to lower the computational efforts when considering a large number of contingencies.

In future work, the proposed model can be used to analyze the congestion management with distributed renewable generators in the system. The comparison of ac and soc formulation can also be carried out for stressed conditions of the system.

ACKNOWLEDGMENT

This work is supported by the project HVDC Inertia Provision (HVDC Pro), financed by the ENERGIX program of the Research Council of Norway (project number 268053/E20) and the industry partners: Statnett, Equinor, RTE, and ELIA.

REFERENCES

[1] TYNDP 2020 introduction and highlights — ENTSOG & ENTSO-e. [Online]. Available: https://2020.entsos-tyndp-scenarios.eu/

[2] ENTSOs system needs - TYNDP. [Online]. Available: https://tyndp.entsoe.eu/system-needs/

[3] "European commission: Commission regulation (EU) 2015/1222 establishing a guideline on capacity allocation and congestion management," *Official Journal of the European Union*, July (2015).

[4] S. Dutta and S. P. Singh, "Optimal rescheduling of generators for congestion management based on particle swarm optimization," *IEEE Transactions on Power Systems*, vol. 23, no. 4, pp. 1560–1569, 2008.

[5] J. Han and A. Papavasiliou, "Congestion management through topological corrections: A case study of central western europe," *Energy Policy*, vol. 86, pp. 470–482.

[6] F. Capitanescu, M. Glavic, D. Ernst, and L. Wehenkel, "Applications of security-constrained optimal power flows," in *Modern Electric Power Systems Symposium, MEPS06*, p. 7.

[7] M. M. Esfahani, M. H. Cintuglu, and O. A. Mohammed, "Optimal real-time congestion management in power markets based on particle swarm optimization," in *2017 IEEE Power Energy Society General Meeting*, 2017, pp. 1–5.

[8] L. Roald, S. Misra, T. Krause, and G. Andersson, "Corrective control to handle forecast uncertainty: A chance constrained optimal power flow," *IEEE Transactions on Power Systems*, vol. 32, no. 2, pp. 1626–1637, 2017.

[9] K. Baker, "Solutions of DC OPF are never AC feasible," *Proceedings of the Twelfth ACM International Conference on Future Energy Systems*, 2021.

[10] D. Van Hertem, J. Verboomen, K. Purchala, R. Belmans, and W. Kling, "Usefulness of DC power flow for active power flow analysis with flow controlling devices," in *The 8th IEE International Conference on AC and DC Power Transmission*, 2006, pp. 58–62.

[11] S. H. Low, "Convex relaxation of optimal power flow—part I: Formulations and equivalence," *IEEE Transactions on Control of Network Systems*, vol. 1, no. 1, pp. 15–27, 2014.

[12] R. Jabr, "Radial distribution load flow using conic programming," *IEEE Transactions on Power Systems*, vol. 21, no. 3, pp. 1458–1459, 2006.

[13] Z. Yuan and M. R. Hesamzadeh, "Second-order cone AC optimal power flow: convex relaxations and feasible solutions," *Journal of Modern Power Systems and Clean Energy*, vol. 7, no. 2, pp. 268–280, 2019.

[14] M. Baradar, M. R. Hesamzadeh, and M. Ghandhari, "Second-order cone programming for optimal power flow in VSC-type AC-DC grids," *IEEE Transactions on Power Systems*, vol. 28, no. 4, pp. 4282–4291, 2013.

[15] H. Ergun, J. Dave, D. Van Hertem, and F. Geth, "Optimal power flow for AC–DC grids: Formulation, convex relaxation, linear approximation, and implementation," *IEEE Transactions on Power Systems*, vol. 34, no. 4, pp. 2980–2990, 2019.

[16] J. Bezanson, A. Edelman, S. Karpinski, and V. B. Shah, "Julia: A fresh approach to numerical computing," *SIAM Review*, vol. 59, no. 1, pp. 65–98, 2017.

[17] I. Dunning, J. Huchette, and M. Lubin, "Jump: A modeling language for mathematical optimization," *SIAM Review*, vol. 59, no. 2, pp. 295–320, 2017.

[18] C. Coffrin, R. Bent, K. Sundar, Y. Ng, and M. Lubin, "Powermodels. jl: An open-source framework for exploring power flow formulations," in *2018 Power Systems Computation Conference (PSCC)*, 2018, pp. 1–8.

[19] F. Geth, "PowerModelsReliability.jl," original-date: 2017-08-29T08:57:59Z. [Online]. Available: https://github.com/frederikgeth/PowerModelsReliability.jl

[20] M. Bynum, A. Castillo, J.-P. Watson, and C. D. Laird, "Strengthened SOCP relaxations for ACOPF with mccormick envelopes and bounds tightening," in *13th International Symposium on Process Systems Engineering (PSE 2018)*, ser. Computer Aided Chemical Engineering. Elsevier, 2018, vol. 44, pp. 1555–1560.

[21] V. Bhardwaj, H. Ergun, and D. Van Hertem, "Risk-based preventive-corrective security constrained optimal power flow for ac/dc grid," in *2021 IEEE Madrid PowerTech*, 2021, pp. 1–6.

[22] C. Coffrin, H. L. Hijazi, and P. Van Hentenryck, "The QC relaxation: A theoretical and computational study on optimal power flow," *IEEE Transactions on Power Systems*, vol. 31, no. 4, pp. 3008–3018, 2016.

[23] G. P. McCormick, "Computability of global solutions to factorable nonconvex programs: Part I — convex underestimating problems," *Mathematical Programming*, vol. 10, pp. 147–175.

[24] C. Coffrin, H. L. Hijazi, and P. Van Hentenryck, "Strengthening the SDP Relaxation of AC Power Flows With Convex Envelopes, Bound Tightening, and Valid Inequalities," *IEEE Transactions on Power Systems*, vol. 32, no. 5, pp. 3549–3558, Sep. 2017.

[25] IEEE 118-bus system, electrical and computer engineering department, illinois institute of technology. [Online]. Available: http://motor.ece.iit.edu/data/

[26] L. Roald, T. Krause, and G. Andersson, "Integrated balancing and congestion management under forecast uncertainty," in *2016 IEEE International Energy Conference (ENERGYCON)*, pp. 1–6.

[27] A. Kaushal, H. Ergun, and D. V. Hertem, "Frequency restoration reserves procurement with hvdc systems," in *The 17th International Conference on AC and DC Power Transmission (ACDC 2021)*, 2021, pp. 155–160.

[28] "D7.3 a broader comparison of different reliability criteria through the GARPUR quantification platform." [Online]. Available: https://www.sintef.no/projectweb/garpur/deliverables/

[29] A. Wächter and L. T. Biegler, "On the implementation of an interior-point filter line-search algorithm for large-scale nonlinear programming," *Mathematical Programming*, vol. 106, pp. 25–57.

[30] Gurobi optimizer reference manual. [Online]. Available: https://www.gurobi.com/documentation/9.1/refman/index.html